Received: 28 February 2024 | Revised: 16 May 2024 | Accepted: 27 May 2024

DOI: 10.1002/bit.28766

ARTICLE

BIOTECHNOLOGY AND BIOENGINEERING WILEY

Lentiviral vector determinants of anion-exchange chromatography elution heterogeneity

George Pamenter[1,2] | Lee Davies[2] | Ciaran Lamont[2] | Danyal Rahim[2] | Carol Knevelman[2] | James Miskin[2] | Kyriacos Mitrophanous[2] | Duygu Dikicioglu[1] | Daniel G. Bracewell[1]

[1]Department of Biochemical Engineering, University College London, London, UK

[2]Oxford Biomedica (UK) Ltd., Oxford, UK

Correspondence
Daniel G. Bracewell, Department of Biochemical Engineering, University College London, London, UK.
Email: d.bracewell@ucl.ac.uk

Funding information
Oxford Biomedica (UK) Ltd.

Abstract

The demand for Lentiviral Vector (LV) drug substance is increasing. However, primary capture using convective anion-exchange chromatography remains a significant manufacturing challenge. This stems from a poor understanding of the complex adsorption behaviors linked to LVs intricate and variable structure, such as high binding heterogeneity which is typically characterized by a gradient elution profile consisting of two peaks. Understanding which LV structural components drive these phenomena is therefore crucial for rational process design. This work identifies the key LV envelope components responsible for binding to quaternary-amine membrane adsorbents. Eliminating the pseudotype protein (Vesicular Stomatitis Virus G glycoprotein [VSV-G]) did not impact the heterogenous two-peak elution profile, suggesting it is not a major binding species. Digestion of envelope glycosaminoglycans (GAGs), present on proteoglycans, leads to a dramatic reduction in the proportion of vector eluted in peak 2, decreasing from 50% to 3.1%, and a threefold increase in peak 1 maximum. Data from reinjection experiments point towards interparticle envelope heterogeneity from discrete LV populations, where the two-peak profile emerges from a subpopulation of LVs interacting via highly charged GAGs (peak 2) along with a weaker binding population likely interacting through the phospholipid membrane and envelope protein (peak 1).

KEYWORDS

capture chromatography, Cell and Gene Therapy, downstream processing, lentiviral purification, lentivirus, viral vector

1 | INTRODUCTION

The rapid rise of Cell and Gene Therapy (C&GT), with the number of clinical trials reaching 1803 in 2023, has sparked a comparative surge in demand for viral-based gene delivery vectors (Alliance for Regenerative Medicine, 2023; Philippidis, 2017). There is a specific need for Lentiviral Vectors (LVs) due to their large genetic capacity and ability to modify both dividing and non-dividing cells (Kim et al., 1998; Mátrai et al., 2010; Naldini et al., 1996). This has made LVs the preferred tool for *ex vivo* modification of patient cells,

particularly in Chimeric Antigen Receptor T-cell (CAR-T) therapies (Milone & O'Doherty, 2018). However, the industry faces challenges in manufacturing these advanced therapeutics which has contributed to a restricted global supply of drug product, limited patient access and low early line usage (Srivastava & Foster, 2023). As CAR-T developers continue to progress new technologies that enhance therapy accessibility, efficacy and safety, the demand for high quality LV products is only set to rise (Beam Therapeutics, 2023; Castelli et al., 2022; Verma et al., 2023; Xin et al., 2022). The manufacture of LV raw material is a major bottleneck, with low cell culture titers (~10^6–10^8 TU/mL) compounded by overall yields of 15–25% in downstream processing (Comisel et al., 2021; Masri et al., 2019). Advances in purification science are therefore crucial to increase the availability of LV drug substance.

Third generation LVs, based on Human Immunodeficiency Virus Type 1 (HIV-1), are 80–120 nm in size and comprised of a ssRNA genome encased in a capsid p24 protein shell which is further enveloped in a phospholipid membrane derived from the production cell. This envelope is formed during the budding process and adds further structural complexity as it contains a variety of species inherent to the production cell membrane, which afford LVs a net negative charge at neutral pH (Nguyen & K Hildreth, 2000; Rodrigues et al., 2008) (Figure 1a). Charge-based separation using anion-exchange chromatography (AIEX) is therefore widely applied for primary product capture in LV bioprocessing, but inconsistent performance is reported in the literature, with LV losses typically ranging from ~60–80% at large scale (Moreira et al., 2021; Valkama et al., 2020). This inconsistency arises from a poor understanding of the complex adsorption behaviors underpinning LV AIEX, leading to an empirical approach to process development. Recent work has employed high-throughput techniques to analyze LV AIEX, examining the impact of pH, buffer mobile phase, and resin type on overall LV AIEX recovery in bead-based adsorbents (Ghosh et al., 2022). Our prior work also demonstrated that LV AIEX binding involves complex time-dependent sorption behavior on solid-phase adsorbents, with significant binding heterogeneity that is characterized by a broad, two-peak, salt gradient elution profile consisting of weak (peak 1, ~400 mM NaCl) and strong (peak 2, ~900 mM NaCl) binding peaks (Pamenter et al., 2023). Understanding which LV structural components drive these behaviors is crucial for further rational design of this unit operation.

Heterogeneous elution profiles are often assumed to result from variations in envelope protein density (Perry & Rayat, 2021; Rodrigues et al., 2008). LVs with higher amounts of envelope protein are expected to elute at higher salt concentrations due to increased multipoint attachment, as Rodrigues et al., 2008 demonstrated that Retroviral Vectors (RVs) eluted at higher conductivities possessed a higher ratio of gp70 (SU protein) to capsid protein. During LV production, the vector is pseudotyped with an artificial envelope protein derived from another virus to mediate receptor recognition with the desired target cell. Vesicular Stomatitis Virus G glycoprotein (VSV-G) is widely used as a viral pseudotype due to its broad tropism and stability in LV bioprocessing (Perry & Rayat, 2021). As VSV-G is highly expressed and contains a theoretical negative charge at neutral pH (calculated protomer ectodomain pI = 5.45, UniProt, 2024) variations in VSV-G envelope density could drive heterogeneous binding on AIEX adsorbents. However, the role of VSV-G expression in LV AIEX binding has never been explored despite the extensive use of the pseudotype.

We hypothesize that the bimodal nature of the two-peak profile suggests two distinct modes of interaction. As previous work has already ruled out the ssRNA genome as an AIEX binding determinant, interactions are likely driven by separate components of the envelope (Yamada et al., 2003). Examples of two separate binding modes could be via phospholipid membrane or envelope proteins. However, the full complexity of the membrane glycocalyx (an external brush-like layer of glycoprotein, glycolipid and proteoglycan present on the cell membrane) is often not considered in the context of charge-based separations (Figure 1a), yet its importance is frequently documented in the field of extracellular vesicles (EVs) in terms of particle function (Gerlach & Griffin, 2016; Zheng et al., 2022).

Proteoglycans, such as syndecans and glypicans (Figure 1a), are of particular interest owing to the long polysaccharides known as glycosaminoglycans (GAGs) that are bonded to the core protein unit (Couchman & Pataki, 2012). These GAGs possess a strong negative charge due to the presence of sulfated groups and are ubiquitous across all human cell surfaces, including the HEK293 cells used for LV production (Bausch-Fluck et al., 2015; Lee et al., 2016; Shi et al., 2021). Heparan Sulfate (HS) and Chondroitin Sulfate (CS) are two of the most commonly occurring GAGs in membrane-associated proteoglycans and are thus transferred to the LV envelope during the budding process (Couchman & Pataki, 2012). We hypothesize that these species participate in LV AIEX binding as their highly-charged long-chain nature makes them prime candidates for forming strong multipoint interactions with AIEX ligands. We previously reported loss of LV recovery due to complex multistate binding, wherein extended periods in the bound state lead to increasing multipoint attachment of LV that results in a transition of peak 1 and 2 to an irreversibly bound population that can only be eluted with NaOH (CIP Peak, Figure 1b) (Pamenter et al., 2023). GAGs, as highly-charged, long-chain polymers, could also contribute to this loss mechanism due to the ability to form strong avidity interactions.

Interaction with discrete components of the LV membrane could result in the emergence of a two-peak profile by two separate mechanisms. Individual peaks could arise from separate LV populations each possessing different binding species on their envelope (interparticle envelope heterogeneity) (Figure 1b,i). Alternatively, LVs with multiple binding domains on one LV surface could cause two peaks by a purely stochastic process, where the binding species is dictated by the orientation of vector upon surface interaction (intraparticle envelope heterogeneity) (Figure 1b,ii). Similar multistate binding has been suggested for purification of proteins during AIEX (Diedrich et al., 2017).

In this work, quaternary-amine derivatised membrane adsorbers (Q-membranes) are employed to assess the impact of VSV-G

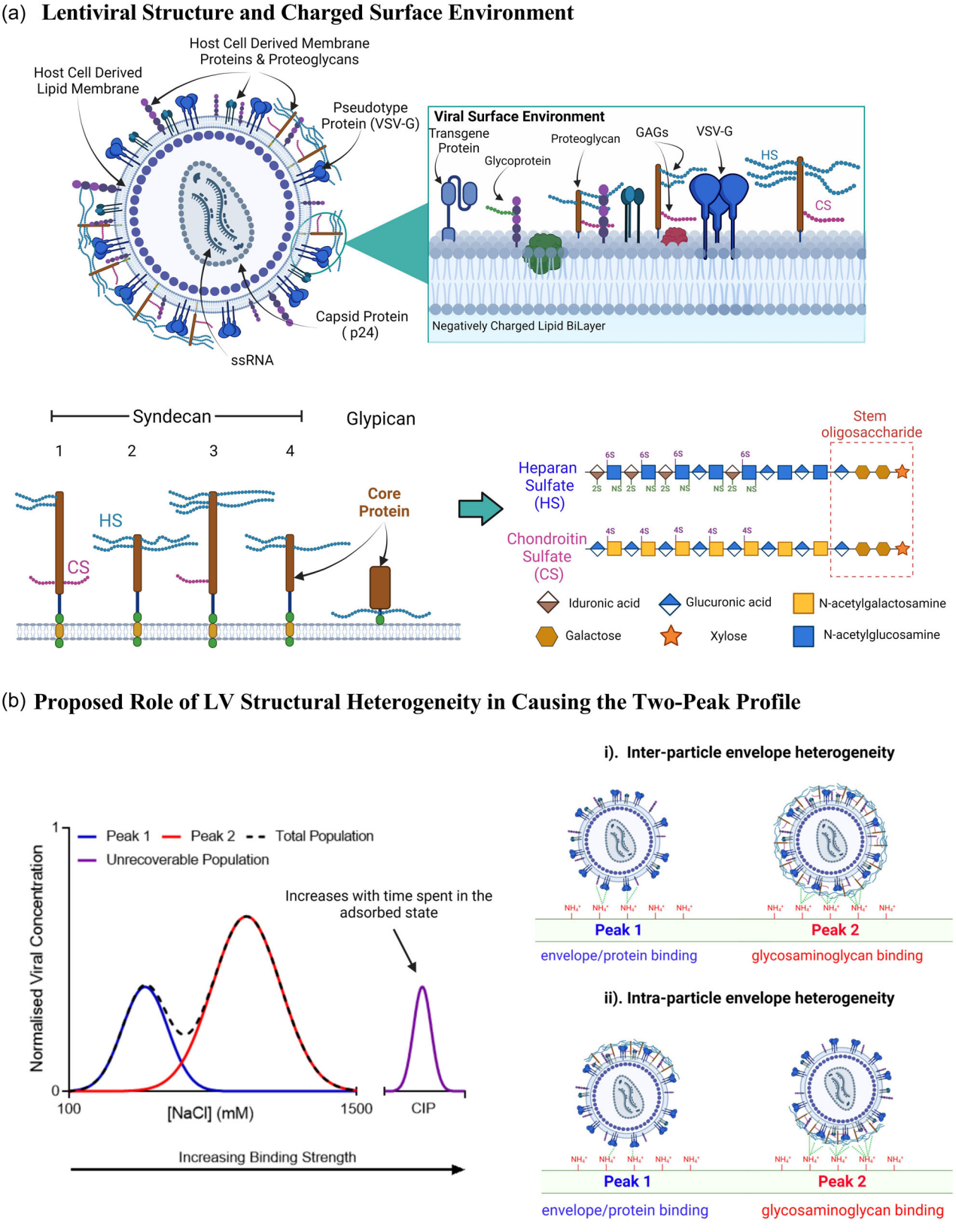

FIGURE 1 Schematic view of the Lentiviral Vector (LV) envelope environment and its hypothesized role in defining binding heterogeneity over AIEX adsorbents. (a) Representation of LV structure and envelope environment including a schematic of some common membrane proteoglycans alongside the generic structure of the glycosaminoglycans (GAGs) Heparan Sulfate (HS) and Chondroitin Sulfate (CS). Proteoglycan and GAG schematics were adapted from information in Binch et al. (2016) and Couchman and Pataki (2012). (b) Proposed mechanism by which variations in LV structure could give rise to the observed two-peak elution profile. (i) Interparticle envelope heterogeneity from discrete LV binding populations. (ii) Intraparticle envelope heterogeneity giving multiple binding patches on similar LV.

expression on LV recovery and elution heterogeneity. LV constructs devoid of envelope VSV-G are used in a series of enzymatic digestion experiments to identify the envelope species impacting the two-peak profile. Protease digestion of LV envelope components is first used to understand the holistic role of the envelope proteome in vector binding. Specific HS and CS digesting enzymes elucidate the role of each GAG species in LV binding. GAG digestion is then conducted on functional LV containing VSV-G in the envelope to see whether similar effects are observed. Contact time experiments are then used to assess whether GAGs contribute to loss of LV recovery with time spent in the adsorbed state. Finally, to discern if the two-peak profile stems from inter- or intraparticle envelope heterogeneity, peak 1 and peak 2 material is isolated and reinjected onto new Q-membranes to see whether a two-peak profile is re-established in the individual peak materials.

2 | MATERIALS AND METHODS

2.1 | Cell culture and clarification

Third-generation HIV-1 LVs, carrying a GFP transgene, were generated using the same upstream cell culture method as detailed in (Pamenter et al., 2023). Three production modes—24 deep-well plates (24DWP), 250 mL shake flasks (SFs) (Erlenmeyer), and 7 L stirred tank bioreactors (STRs) (Applikon)—were employed. 24DWP and SFs were maintained in a shaking incubator at 300 and 190 rpm, with cell culture material harvested through centrifugation and 0.45 µm syringe filtration, giving clarified cell culture harvest (CCH). LV production in 7 L STRs is detailed in (Pamenter et al., 2023). All CCH was stored at −80°C before AIEX experiments. AIEX experiments with STR-derived CCH feed utilized a single STR batch (Sections 3.5–3.10). All other AIEX experiments used CCH derived from 250 mL SF (Sections 3.2–3.4).

2.2 | Anion-Exchange chromatography

Frozen CCH was thawed rapidly at 37°C in a water bath before chromatography. An ÄKTA Avant 150 (Cytiva) and Sartobind® Q Nano 1 mL or Sartobind® Q Pico 0.08 mL membrane adsorbers (Sartorius) were used depending on the experimental design. Two process buffers were used with both formulated in 20 mM Tris, pH 7.2, at two NaCl concentrations (Buffer A = 150 mM, Buffer B = 2000 mM). Before material introduction, flow paths and membranes underwent 0.5 M NaOH decontamination, followed by charging (Buffer B) and equilibration (Buffer A). The same ÄKTA method was applied for all Sartobind® Q experiments unless otherwise stated. 300 CV of CCH was loaded at 12.5 CV/min. Sample injection concluded with a 40 CV Buffer A flush. Gradient elutions were conducted by mixing process buffers on the AKTA from 150 to 1350 mM (0–64.9% Buffer B) at a reduced flow rate of 6.25 CV/min and a gradient length of 300 CV for high UV resolution. 15 sample fractions were collected (100 mM steps). The salt composition of each fraction was confirmed offline using the Orion Star™ A211 Benchtop pH/Conductivity Meter (Thermo Fisher Scientific) on a test gradient method. For all experiments using functional vectors, fractions were diluted 1:1 in a 0 mM NaCl buffer.

2.3 | Generating peak material and AIEX reinjection experiments

Sartobind® Q Nano 1 mL membranes were used to generate high titer material from peak 1, transition and peak 2 (Figure 6d) by first loading 300 CV of CCH at a high flow rate (30 CV/min) to minimize time-dependent losses. This was followed by a 30 CV Buffer A flush and 15 CV step elutions at 450 mM (16.2% Buffer B), 825 mM (36.5% Buffer B), and 1350 mM (64.9% Buffer B). A reduced elution flow rate of 5 CV/min ensured complete capture of the elution peak in 15 CV. Samples were all diluted to 150 mM NaCl using 0 mM NaCl buffer to achieve a uniform salt environment of each peak for reinjection. This was conducted three times to generate peak material in triplicate. The gradient control followed the same protocol, but with a linear gradient elution (150–1350 mM NaCl) over 60 CV with an elution flow rate of 10 CV/min. All fractions were diluted 1:1 in 0 mM NaCl buffer. All eluted peak material was re-injected onto a Sartobind® Q nano 1 mL at 65 CV/min, to further reduce time-dependent losses, and then subject to the same gradient elution as above.

2.4 | Contact time experiments

To generate kinetic profiles of LV loss with time spent in the adsorbed state we implemented a similar protocol as described previously in Pamenter et al. (2023), but adapted for smaller Sartobind® Q Pico 0.08 mL membranes that were required due to enzyme availability. Columns were underloaded with 60 CV of CCH using a twofold underfilled sample loop at 65 CV/min. Sample application, and membranes flushing, was completed with 15 mL of Buffer A. Static, on-column, incubations following this Buffer A flush were implemented to generate average times spent in the adsorbed state of 3.5 min (0 min incubation), 12.5, 25, 50, and 100 min (96.5 min incubation). Isocratic elutions were then performed using 5 mL (62.5 CV) of 1350 mM NaCl Buffer (64.9% Buffer B) and diluted 1:1 in 0 mM NaCl buffer.

2.5 | TrypLE™, heparinase I/III and chondroitinase ABC digestions

TrypLE™ select 10X (Gibco™), a trypsin-like serine protease, was used for digestion of LV membrane proteins, as serine proteases have

been demonstrated for similar applications in RVs (Rodrigues et al., 2008). TrypLE™ (Tryp) was added to 24 mL of CCH material to achieve concentrations of 0.05X, 0.25X, and 0.45X, followed by a 1 h incubation at room temperature. The enzyme conditions were chosen based on prior LV product experience and literature, where 0.05% trypsin treatment was effective in digesting most envelope proteins (Dautzenberg et al., 2021).

To digest HS and CS, two enzymes were used. A blended Heparinase I/III (Sigma-Aldrich, Merck) was used for optimal HS digestion. Chondroitinase ABC (Sigma-Aldrich, Merck) was selected for CS removal but also displays activity towards Dermatan Sulfate (Couchman & Pataki, 2012). Enzyme stock solutions (20 U/mL) were prepared on the experiment day using FreeStyle 293 Expression Media (Thermo Fisher Scientific), not buffer, to maintain a representative mobile phase. These solutions were added to 24 mL of CCH at a target concentration of 0.8 U/mL and incubated at 37°C for 1 h. 0.8 U/mL was chosen to give a substantial excess based on previous internal work with these enzymes. Material was then equilibrated to room temperature for 1 h before AIEX load. Control samples underwent the same procedure in the absence of enzyme.

2.6 | Functional vector and p24 concentration measurement

Functional titer was determined following the method outlined in Pamenter et al., 2023. Briefly, samples were diluted in DMEM Media (Sigma-Aldrich, Merck) supplemented with polybrene (Sigma-Aldrich, Merck) and added in duplicate or triplicate, depending on assay size, to adherent HEK293T cells. Cell analysis was performed using an Attune NxT acoustic focusing flow cytometer (Thermo Fisher Scientific), collecting size and GFP fluorescence data to determine the percentage of cells exceeding the background fluorescence of non-transduced cells. GFP titer was calculated by Equation (1):

$$\text{Titer}\left(\frac{\text{TU}}{\text{mL}}\right) = \frac{[\%\ \text{cells expressing GFP} \times \text{number of cells at transduction} \times \text{dilution factor}]}{\text{Volume of Vector added at transduction}} \quad (1)$$

HIV-1 p24 concentration was measured via the Ella™ (Protein Simple) high-throughput automated HIV-1 p24 enzyme-linked immunosorbent assay (ELISA), developed in-house by the Oxford Biomedica Process Research and Development Analytics team in collaboration with the manufacturer.

For measurement of T cell functional vector activity, Peripheral Blood Mononuclear Cells (PBMCs) within the Oxford Biomedica PBMC bank, isolated with Leukapheresis from two donors subsequently referred to here as Donor 1 and Donor 2, were employed in this study. Diluted vector samples were added to the cells at an multiplicity of infection (MOI) of 0.5. Analysis was performed on a Fortessa X-20 flow cytometer (BD Biosciences).

2.7 | Total particle recovery and relative activity calculation

Due to variations in LV AIEX flowthrough quantity across conditions (e.g. from differences in "free" p24 not associated with vector), analysis focused solely on the recovery of material actually bound to the membrane to better comprehend differences in membrane elution behavior. Consequently, the membrane mass balance yields Equation (2) for total particle recovery. The relative activity of vector material is determined by the functional titer to p24 ratio, Equation (3):

$$\text{Total Particle Recovery} = \frac{\text{Eluted p24 Mass (pg)}}{\text{Total Loaded p24 mass (pg)} - \text{Flow through p24 mass (pg)}} \quad (2)$$

$$\text{Relative Activity}\left(\frac{\text{TU}}{\text{pg}}\right) = \frac{\text{Functional Titer}\left(\frac{\text{TU}}{\text{mL}}\right)}{\text{p24}\left(\frac{\text{pg}}{\text{mL}}\right)} \quad (3)$$

2.8 | Particle size measurement and VSV-G Western blot

Particle size distributions were measured using a Zetasizer Nano (Malvern Scientific) Dynamic Light Scattering (DLS) machine. Measurements analyzed 100 µL of sample at 20°C using a 633 nm laser and detecting backscattered light at an angle of 173°.

VSV-G concentration was qualitatively assessed through Western blots. Initial SDS-PAGE analysis involved using 45 µL of sample and 15 µL of 4X Laemmli Sample Buffer (Bio-Rad), boiled at 95°C for 5 min. Samples were then loaded onto a 4–20% Criterion™ TGX™ Precast Midi Protein Gel (Bio-Rad) and run at 40 mA/gel constant amperage in Running Buffer. Proteins were transferred onto a nitrocellulose membrane using the Trans-Blot® Turbo™ RTA Mini Nitrocellulose Transfer Kit (Bio-Rad). Membranes were then blocked in 5% milk for at least 1 h. Primary antibodies were diluted in 5% milk and incubated at 4°C overnight. Secondary antibodies were diluted in 5% milk and added to the membrane for a 2 h incubation at room temperature. Membranes were visualized using the Western blot analysis Detection Reagents (GE HealthCare Amersham™ ECL™) and imaged on the ChemiDoc Imager (Bio-Rad). A VSV-G Tag Polyclonal Antibody was used. VSV-G band intensity was calculated using Image Lab software (Bio-Rad).

2.9 | Statistics, nonlinear regression and model fitting

Hypothesis testing was conducted using JMP® 16 statistical software (SAS). Significance is given at the $\alpha_{0.05}$ level unless otherwise stated. We previously described a model for estimating the p24 mass in each elution peak of the two-peak profile, wherein the overall concentration profile was defined as the additive effect of two

skewed-Gaussian populations, each representing a single peak in the elution profile (Equation 4). A detailed description can be found in (Pamenter et al., 2023). Nonlinear regression was performed using the "scipy. optimize. curve_fit" package in Python.

$$q_1 = \frac{B_1\varphi(X_1)\cdot 2\Phi(\alpha_1 X_1)}{\Phi(0)} + \frac{B_2\varphi(X_2)\cdot 2\Phi(\alpha_2 X_2)}{\Phi(0)} \quad (4)$$

Where q_1 = eluted viral concentration (p24 μg/mL), $B_{1,2}$= peak magnitude coefficient (μg), $s_{1,2}$= peak 1/2 standard deviation (mL), $m_{1,2}$= peak 1/2 mean (mL), x= volume (mL), $\alpha_{1,2}$ = skewness factor and $\Phi(0)$ = cumulative distribution function at $\alpha_{1,2}$ = 0.

2.10 | Sulphated GAG concentration measurement

The concentration of sulphated GAGs was quantified using a "Sulphated Glycosaminoglycan Detection Kit" (AMS Biotechnology) with the metachromatic dye capable of detecting various sulphated GAGs but without distinguishing species. These include chondroitin-4-sulphate, chondroitin-6-sulphate, dermatan sulphate, heparan sulphate, heparin, and keratin sulphate. The kit was utilized as per the manufacturer's instructions and plates measured at 525 nm using a SpectraMax® i3x spectrophotometer (Molecular Devices LLC).

3 | RESULTS AND DISCUSSION

3.1 | Production of LV possessing varying amounts of VSV-G envelope protein

Previous work has suggested increased envelope protein density results in stronger binding of RVs to AIEX adsorbents due to increased multipoint attachment (Rodrigues et al., 2008). As such, VSV-G is a potential candidate for driving LV binding as the protomer ectodomain has a theoretical pI = 5.45 and high expression levels are required for transduction capable vectors (Farley et al., 2007; UniProt, 2024). The role of VSV-G in LV binding was explored by first manipulating cell culture transfection conditions to generate LV constructs with varying levels of VSV-G envelope expression, then assessing each construct on AIEX.

As the expression level of VSV-G in the production cell membrane is directly related to that of the budded vector, to determine the amount of pVSV-G required to generate LV with an intermediary VSV-G content, upstream 24DWP screening studies were conducted with pVSV-G concentrations ranging from 0.07 μg/mL (100%) to 0 μg/mL (0%) based on work by Farley et al., 2007 (Figure 2). Functional titer increased from 0 TU/mL (0% pVSV-G) to ≈ 1.7×10^7 TU/mL at 50% pVSV-G with no further increase at 100% pVSV-G (Figure 2c). A similar trend in VSV-G expression was confirmed by Western blot with a small decline in cell culture viability at harvest also observed at increased pVSV-G as expected (Figure 2a,b). The condition generating LV with 50% of the maximum functional titer (9.00×10^6 TU/mL) was selected as the intermediary VSV-G expression level (pVSV-G = 12.5%). This also corresponds to an approximate halving of the average VSV-G band intensity (2.5-fold reduction) measured by Western blot (Figure 2b). To confirm the presence of vector particles at 0% VSV-G, we checked for particles in the vector size range by DLS (Figure 2d). No difference in particle size between fully functional vectors (100% pVSV-G) and VSV-G deficient vectors (0% pVSV-G) was observed.

3.2 | The role of the VSV-G pseudotype protein expression on AIEX elution

Using the 0, 12.5 and 100% materials generated in Section 3.1, experiments were performed to investigate the impact of VSV-G envelope concentration on AIEX elution. 300 CV of thawed CCH was loaded onto Q-membranes, followed by a 150–1350 mM NaCl linear gradient elution. Representative chromatograms are given in Figure 3a,b. AIEX performance was primarily analyzed by capsid protein p24 ELISA due to the lack of functionality at pVSV-G = 0%. Cumulative recoveries were calculated from the sum of all eluted fractions (Figure 3c). Each pVSV-G condition led to differences in CCH p24 concentration and the amount of "free" p24 observed in the AIEX flowthrough. Analysis of p24 concentration during elution would therefore give a biased view of elution performance. To more accurately compare adsorption behavior of LV particles actually bound to the column, total particle recovery (recovery of bound material only, see Section 2.7) is reported. No significant difference in total particle recoveries occurred with reduction of pVSV-G expression from 100% pVSV-G (recovery = 41%) to 12.5% pVSV-G (40%) and 0% pVSV-G (47%). Cumulative functional titer recovery was also unaffected by reducing pVSV-G from 100% to 12.5% (TU recovery = 12%) indicating no significant changes in general AIEX performance.

We previously reported that LV elute in a characteristic two-peak profile during gradient elution. As previous work by Rodrigues et al. (2008) has suggested the importance of envelope proteins in defining binding of RV to AIEX adsorbents, it is often assumed that VSV-G plays a significant role in LV binding heterogeneity due to its high abundance in the LV envelope and potential for variable expression. The total particle elution profiles at each VSV-G expression level were however surprisingly similar, with the characteristic two-peak profile observed at all pVSV-G concentrations (Figure 3d). Notable changes to the distribution of LV material between the two peaks are also observed, with a 2.1-fold increase in total particle peak 1 maximum occurring from 4.0% (100% pVSV-G) to 8.4% (0% pVSV-G). This increase in peak 1 maximum could be due to increased lipid membrane interaction as the envelope is likely more exposed, and therefore accessible for binding, in the absence of VSV-G. Nevertheless, these data indicate that the pseudotype protein VSV-G is not the primary contributor to LV AIEX binding.

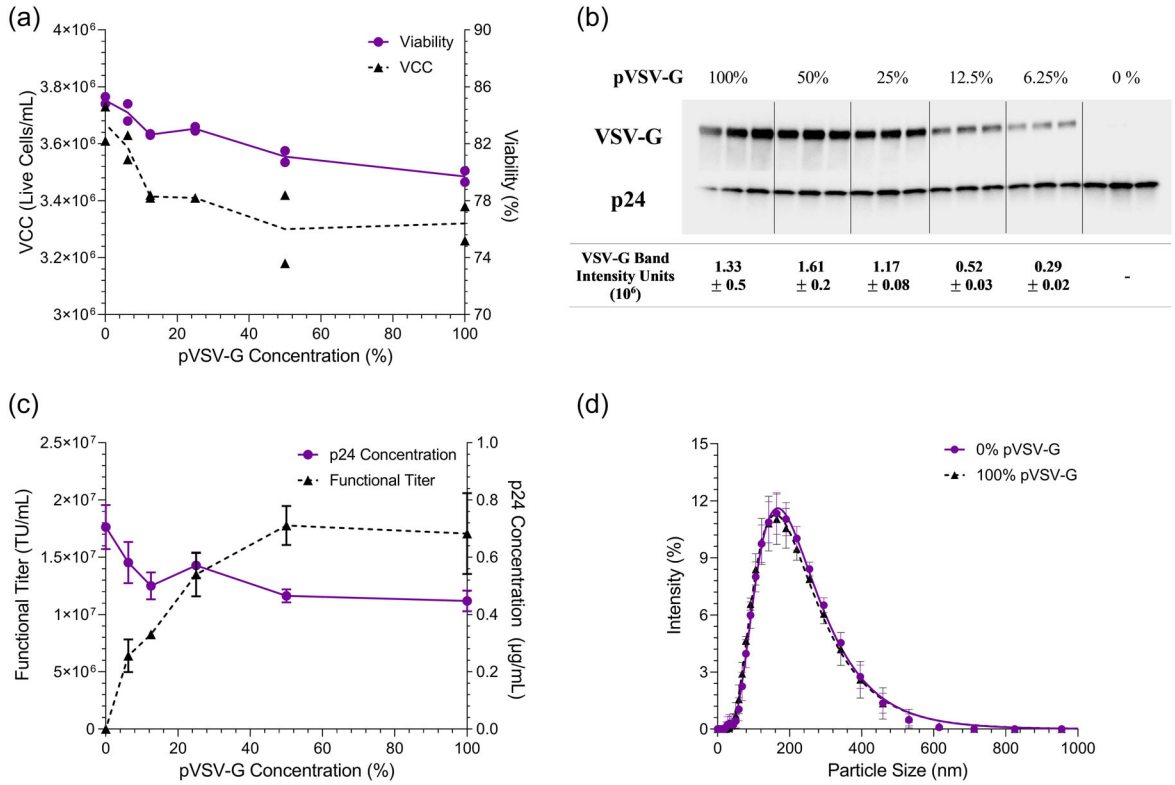

FIGURE 2 Production of LV containing various levels of Vesicular Stomatitis Virus G glycoprotein (VSV-G) expression on the viral envelope. (a) Impact of cell culture pVSV-G concentration on viable cell concentration (VCC) and viability at harvest. Individual runs are shown for the two cell count wells in the 24DWP. (b) Western blot analysis indicating the impact of culture pVSV-G on total expression of VSV-G and p24 in the clarified cell culture harvest (CCH). Columns contain biological triplicates. Average VSV-G band intensity is given on figure alongside ±1 SD. (c) Impact of pVSV-G concentration on functional titer and p24 concentration in the CCH. Error bars represent ±1 SD at $N = 6$ biological replicates for functional titer and $N = 3$ biological replicates for p24. (d) Impact of pVSV-G removal on particle size distribution at CCH. No significant difference is seen for 0% and 100% VSV-G.

3.3 | The impact of serine-protease digestion on (−) VSV-G LV elution profiles

As we ruled out VSV-G as a major determinant of the two-peak elution profile, we wished to elucidate the role of the remaining envelope proteins. 0% pVSV-G CCH material, herein referred to as (-) VSV-G, from the same batch as Figure 3 was subject to a Tryp digestion to cleave the remaining envelope proteins and generate "bald" LV particles. Tryp concentrations of 0.05X, 0.25X and 0.45X were explored to see whether a dose-dependent response in the elution profiles could be observed. The same AIEX protocol was used (see Section 2.2). Figure 4a,c give the cumulative recoveries and elution profiles of each Tryp condition alongside (-) VSV-G for use as a control.

Treatment with 0.05X, 0.25X and 0.45X Tryp resulted in reduced load (CCH) p24 concentration from 1.04 µg/mL (control) to 0.87, 0.77 and 0.75 µg/mL respectively. The small reduction in p24 likely results from the degradation of "free" p24 in solution. This is supported by the equivalent reduction in flowthrough p24 recovery from 9.6% (0.05X) to 0.81% (0.45X). As particles in the LV size range were measured at all Tryp concentrations (126 ± 3 nm, data not shown), these data demonstrate that no substantial destruction of LV particles occurred with Tryp addition. No notable difference in cumulative total particle recovery occurred with increasing Tryp concentration (Figure 4a) going from 47% (control) to 40% (0.05X), 41% (0.25X) and 42% (0.45X). However, a dramatic change in the two-peak profile is observed (Figure 4c), with the characteristic two peaks converging to a single tailed peak with the same retention point as peak 1 in the control (≈ 350 mM NaCl). This is characterized by a reduction in the proportion of material eluted above 650 mM NaCl (peak 2) reducing from 46% (control) to 23% (0.05X Tryp), then further to 8% (0.25X) and 9% (0.45X Tryp).

These data appear to further support the hypothesis that binding is bimodal in nature, as one binding mechanism is removed by Tryp action, but another clearly remains. This could be further evidence that peak 1 interaction is governed by the LV membrane as absence of VSV-G and digestion with Tryp in theory generates "bald" vector particles only capable of interacting via the lipid envelope. However, as some envelope protein species display significant resistance to trypsin protease digestion, substantial amounts of envelope protein may remain (Dautzenberg et al., 2021). Thus, it is not possible to differentiate between the role of lipid membrane and remaining envelope proteins in peak 1 binding using just these techniques.

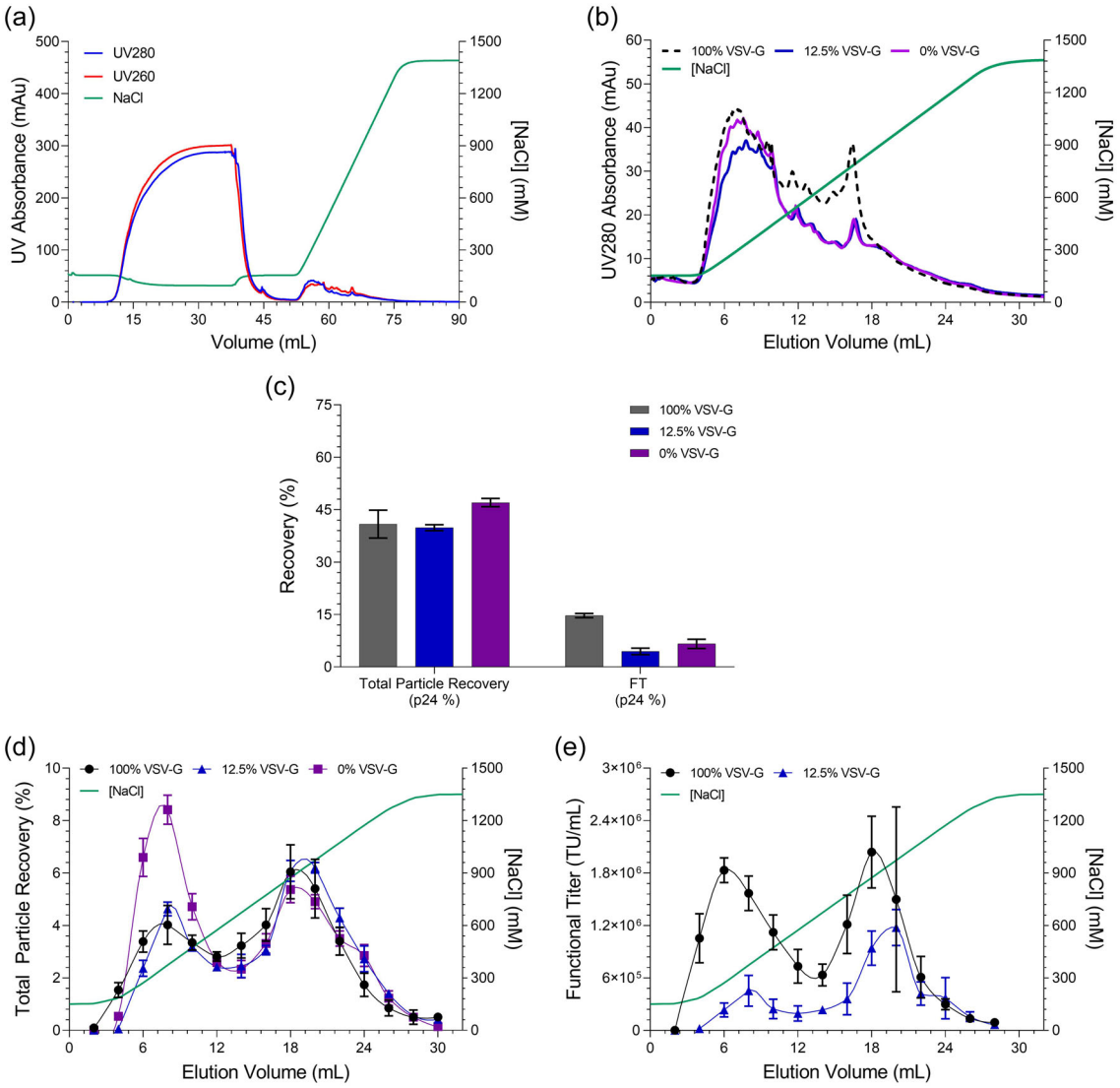

FIGURE 3 Impact of VSV-G expression on elution of LV over Q-membrane adsorbents. Error bars represent ±1 SD at $N = 3$ biological replicates. (a) Representative chromatogram for the complete bind and elute run. The 0% pVSV-G condition is given with load and elution visible. (b) Detailed view of UV280 profile for each pVSV-G condition during gradient elution. Single representative runs are given. (c) Impact of pVSV-G concentration on cumulative recovery and flowthrough (FT). Compared to 100% pVSV-G, no significant difference in total particle recovery is observed for 12.5% ($p = 0.68$) or 0% ($p = 0.063$). (d) Gradient elution profile for total particle recovery. A smoothing spline was used to generate continuous gradient profiles. (e) Gradient elution profile for functional titer. A smoothing spline was used to generate continuous gradient profiles.

However, these data suggest binding of LV within peak 2 is driven by some proteinous species.

3.4 | The role of Glycosaminoglycans in (-) VSV-G LV binding

A literature review of the species contained within the external envelope glycocalyx of HEK293 cells reveals the presence of membrane proteoglycans like syndecan and glypican, which are thus found on budded LVs (Bausch-Fluck et al., 2015; Lee et al., 2016). These proteoglycans, comprising a core protein unit with GAGs attached at various points along them, could engage in strong multipoint interactions with AIEX ligands via these highly charged side-chains (Figure 1). Furthermore, they are also likely removed from LV membranes by Tryp due to cleavage of the core protein unit. The impact of GAG-digesting enzymes targeting the most common species found in membrane proteoglycans was therefore explored using Chondroitinase ABC (digesting CS and Dermatan Sulfate) and Heparanase I/III (digesting HS) (Couchman & Pataki, 2012). It should be noted that Heparanase I/III also exhibits activity towards Heparin. Enzymatic digestion procedures are detailed in Section 2.5, following the same chromatography protocol outlined in Section 2.2. A new LV batch, not containing VSV-G, was produced for this study.

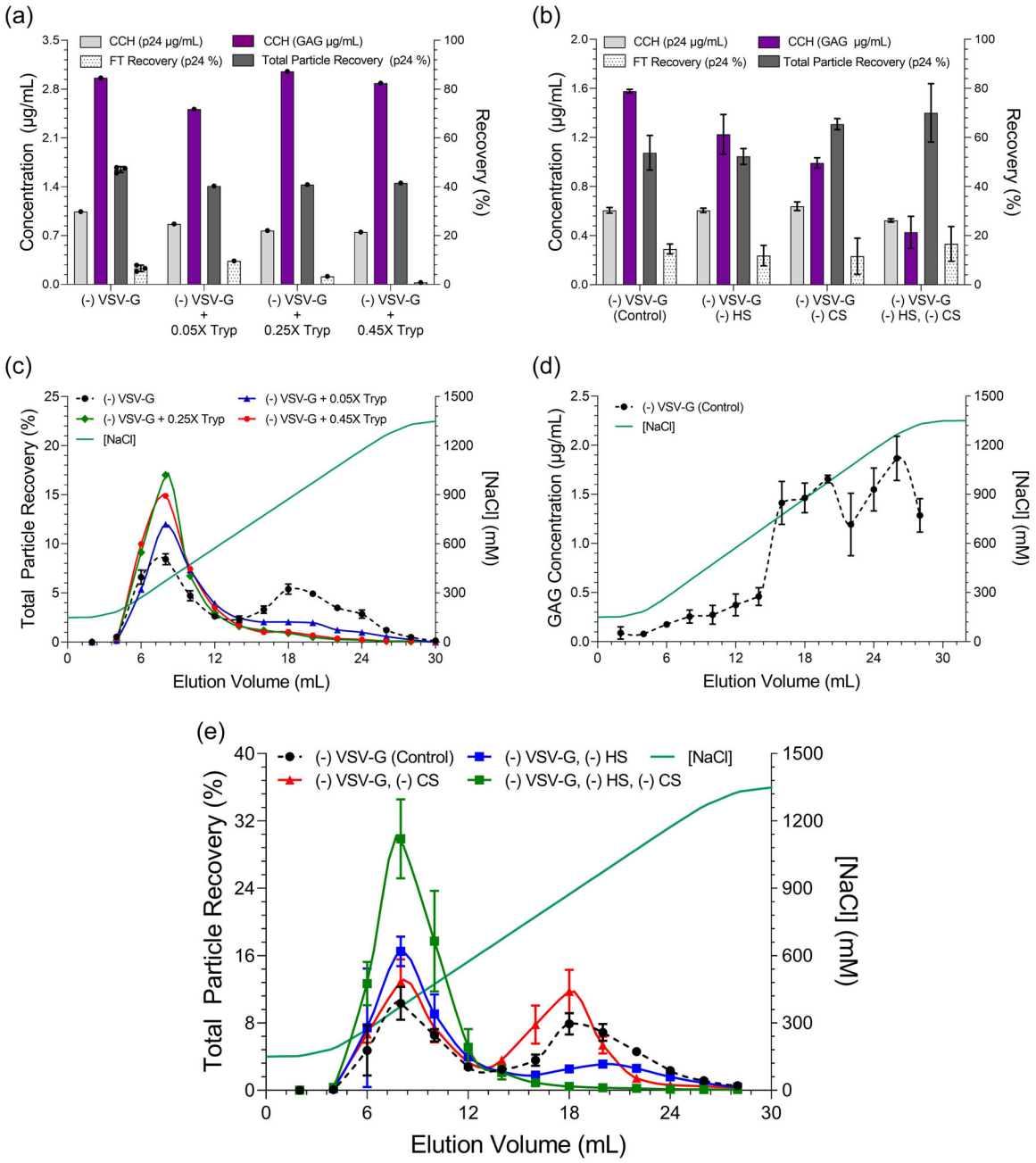

FIGURE 4 Impact of selective digestion of LV envelope species on AIEX elution profiles and overall recovery of LV's not containing VSV-G in the envelope, (-) VSV-G. Error bars represent ±1 SD at $N = 3$ biological replicates unless otherwise stated. (a) Cumulative AIEX recovery for (-) VSV-G LV subject to varying concentrations of TrypLE™ (Tryp). (b) Cumulative AIEX recovery for (-) VSV-G LV with Heparan Sulfate (HS) and Chondroitin Sulfate (CS) removed. Despite increased total particle recovery for (-) CS and the combined digestion, these increases were deemed insignificant ($p = 0.053$ and 0.093 respectively). (c) Impact of Tryp digestion on AIEX elution profiles. 0% pVSV-G data from Figure 3d is replotted to function as the (-) VSV-G control. (d) Concentration of total GAGs eluted during the gradient elution of (-) VSV-G LV. (E) Impact of HS and CS removal on AIEX elution profiles. $N = 4$ biological replicates were conducted for the combined (HS, CS) digestion (green) with error bars representing ±1 SD.

Figure 4b gives the load concentrations and cumulative recoveries of each digestion condition. Similar total particle recovery and flowthrough p24 content is observed across all conditions, indicating that enzymatic digestions did not disrupt the AIEX process. The GAG concentration in the loaded material decreased from 1.6 µg/mL (control) to 0.43 µg/mL upon combined HS and CS removal, thus confirming effective reduction of these species. The elution of all GAG species in the control material was measured (Figure 4d) and shows a broad peak occurs at 650–1350 mM NaCl. This GAG peak co-elutes with LV material in peak 2. This demonstrates that GAG species display similar elution behaviors to LV in peak 2 which could evidence their potential role in binding. However, as a general assay

is used specific species cannot be identified and only the general elution behavior of all GAGs is shown.

A more specific impact of GAG removal on LV binding is visible from the LV total particle elution profiles (Figure 4e). HS digestion led to a large reduction in the proportion of the eluted material obtained above 650 mM (peak 2) reducing from 50% (control) to 25% with a 1.6 fold increase in peak 1 maximum (10% to 16%). CS digestion had less of an impact on LV elution with two peaks still visible and the proportion of eluted material collected above 650 mM similar to that of the control (45%). However, CS digestion does appear to cause a "compression" of the two-peak profile towards lower salt due to a reduction in material eluted at very high NaCl concentrations (~ >1000 mM). Combined digestion had the most significant impact on LV elution, with the characteristic two peaks converging to a single homogenous peak with the same retention as peak 1 in the control. The proportion of material eluted above 650 mM NaCl (peak 2) dramatically reduced from 54% (control) to 3.1% with a threefold increase in peak 1 maximum (10%to 30%). This combined digestion displays notable similarity to that of the 0.45X Tryp condition in Figure 4c.

Combined, Figure 4d,e support the hypothesis that LV binding is driven by separate components of the glycocalyx, where peak 2 arises from interaction with highly charged GAGs. HS appears to contribute to peak 2 binding to a greater extent than CS, as removal of HS led to the largest reduction in peak 2. This is perhaps due to higher prevalence or accessibility of HS due to the structure of common membrane proteoglycans such as syndecan (Binch et al., 2016; Couchman & Pataki, 2012; Iozzo & Schaefer, 2015). One counter hypothesis could be that treatment with individual enzymes results in incomplete digestion due to steric hinderance from other GAG species because of the aforementioned structure of membrane proteoglycans like syndecan. For example, digestion of CS may be hindered by the presence of HS at the outer most part of the proteoglycan. Only upon combined digestion are both species effectively removed thus eliminating any peak tailing. The cause of peak 1 binding is less clear but likely results from interaction with the phospholipid membrane and envelope proteins. This data has relevance to the wider field as similar behaviors may be expected during charge-based separation of any enveloped viruses, VLPs or vesicles.

3.5 | AIEX recovery of functional LV following enzymatic GAG removal

Previously, the role of GAGs in LV adsorption was demonstrated for LVs lacking VSV-G in the envelope. We aimed to further evaluate the effects of GAG digestion on a functional LV containing envelope VSV-G and derived from an STR source to more closely mimic real LV product feedstocks. CCH material (GFP) was subject to combined HS and CS digestion and loaded onto Q-membranes using the same AIEX method (representative chromatogram in Figure 5a).

Figure 5b displays cumulative recovery of total and functional LV particles. Enzyme incubation alone significantly reduced the functional titer of CCH material (TU Recovery = 78%). Given the suggested role of cell surface HS in HIV-1 infection (Connell & Lortat-Jacob, 2013; Vivès et al., 2005), inadvertent digestion of HEK293T cell surface HS from residual GAG enzyme could diminish titers by lowering the susceptibility of assay cells to infection, rather than actual viral activity loss. To address this, we conducted a control by adding untreated CCH to both standard HEK293T cells and cells pretreated with enzyme for 1 h before transduction. This was followed by a media exchange before sample introduction to the assay cells. No difference in functional titer (TU) was detected between the methods (TU recovery = 97%, data not shown), confirming loss of titer due to LV functionality loss.

GAG digestion led to a 2.2-fold increase ($p = 0.005$) in cumulative TU recovery (42%) compared to the control (18%). However, for total particle recovery a smaller 1.4-fold increase was observed (46% and 32%) but deemed insignificant ($p = 0.092$). TU recovery in the flowthrough increased from 1.9% (control) to 8.9%, perhaps indicating a reduction in LV binding strength. Total particle elution profiles (Figure 5c) experienced a similar change as seen in Figure 4e, with the proportion of total particles eluted above 650 mM (peak 2) decreasing from 49% (control) to 19%. A similar reduction was also observed for TU recovery (Figure 5d), reducing from 31% to 10%. This reduction in peak 2 material was less pronounced than for (-) VSV-G vector (Figure 4e), with a notable peak shoulder above 650 mM. This could be due to a less effective GAG digestion due to steric hindrance of envelope GAGs from highly expressed VSV-G. Nevertheless, these data indicate that HS and CS also drive binding of functional LV within peak 2, with a moderate increase in TU recovery achieved upon enzymatic digestion (18% to42%). However, as incubation alone resulted in a significant 22% TU loss, use of GAG enzymes as additives to improve AIEX processes recoveries is not recommended, especially as the impact of this envelope manipulation on LV efficacy is unknown.

3.6 | Time-Dependent sorption behavior of functional LV following enzymatic GAG removal

Our previous findings demonstrated that increased time spent in the adsorbed state reduced LV AIEX recoveries due to growing quantities of irreversibly bound vector from strong avidity interactions (Pamenter et al., 2023). We aimed to explore whether time-dependent product loss of LV on Q-membranes could be mitigated by reducing interaction strength of LV by digestion of the most strongly binding envelope species, namely GAGs. Kinetic profiles for LV recovery with time spent in the adsorbed state, ranging from 3.5 to 100 min, were therefore generated (Figure 5e,f).

Time spent in the adsorbed state strongly impacted LV recovery as previously reported (Pamenter et al., 2023). However, total particle recoveries for control and GAG-digested material displayed near identical loss profiles, reducing from 41% and 40% ($t = 3.5$ min) to 4% and 5% ($t = 100$ min) respectively. A similar trend was observed for functional titer, but at lower recovery. These data indicate that loss of LV to the irreversibly bound state cannot be mitigated by

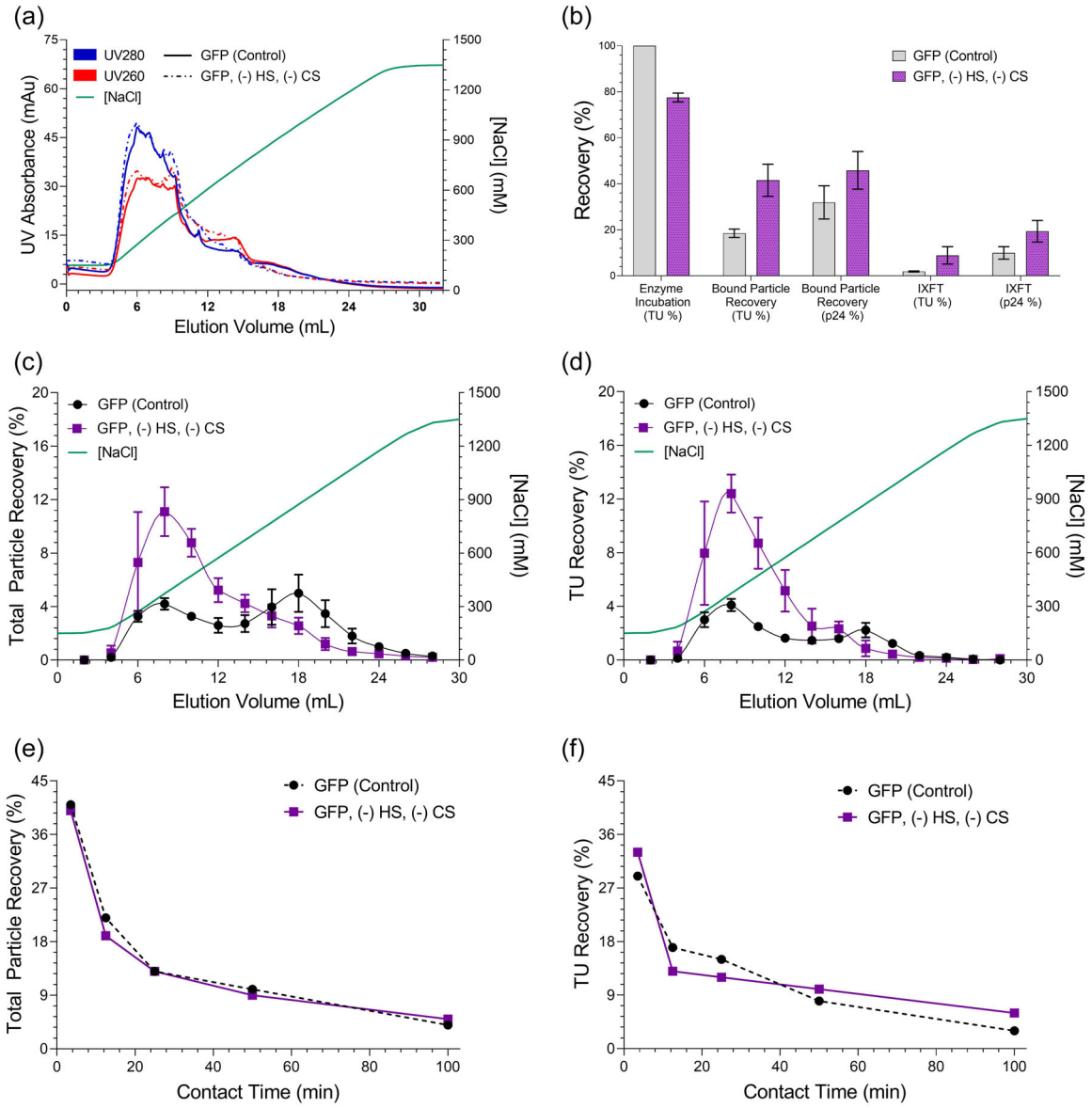

FIGURE 5 The impact of enzymatic GAG removal on elution of functional LV produced in STR. Error bars represent ±1 SD at $N = 3$ biological replicates unless otherwise stated. (a) Representative chromatogram demonstrating the difference in UV elution profiles for the control and GAG digested CCH material. (b) Cumulative recoveries of each process stage obtained from the control and GAG digested material. (c) Comparison of total particle elution profile from the control and GAG digested material. (d) Comparison of functional titer elution profile from the control and GAG digested material. (e) Impact of GAG digestion on the time-dependent loss of total particle recovery. Individual runs are given. (f) Impact of GAG digestion on the time-dependent loss of functional vector recovery. Individual runs are given. CCH, clarified cell culture harvest; GAGs, glycosaminoglycans; STR, stirred tank bioreactors.

digestion of GAG species and aligns with previous findings demonstrating LV loss with time spent in the adsorbed state occurs in both elution peaks (Pamenter et al., 2023).

3.7 | High-resolution fractionation of LV

In the previous experiments, only a relatively low gradient elution fraction resolution (100 mM steps) was used due to analytical loads. This could potentially mask the presence of further sub-peaks in the elution profile. A high-resolution gradient (10 mM steps) was therefore conducted to explore this possibility. Figure 6a demonstrates that two peaks are still obtained even under higher resolution, however more notable difference in peak shape characteristics are observed. Using the skewed-Gaussian model (Section 2.9) a higher degree of skew and lower standard deviation in peak 1 ($\alpha_1 = 5.6$, $s_1 = 5.0$ mL) compared to peak 2 ($\alpha_2 = 0.96$, $s_2 = 7.8$ mL) is measured. This could indicate a greater binding homogeneity in peak 1 compared to peak 2 but requires further investigation.

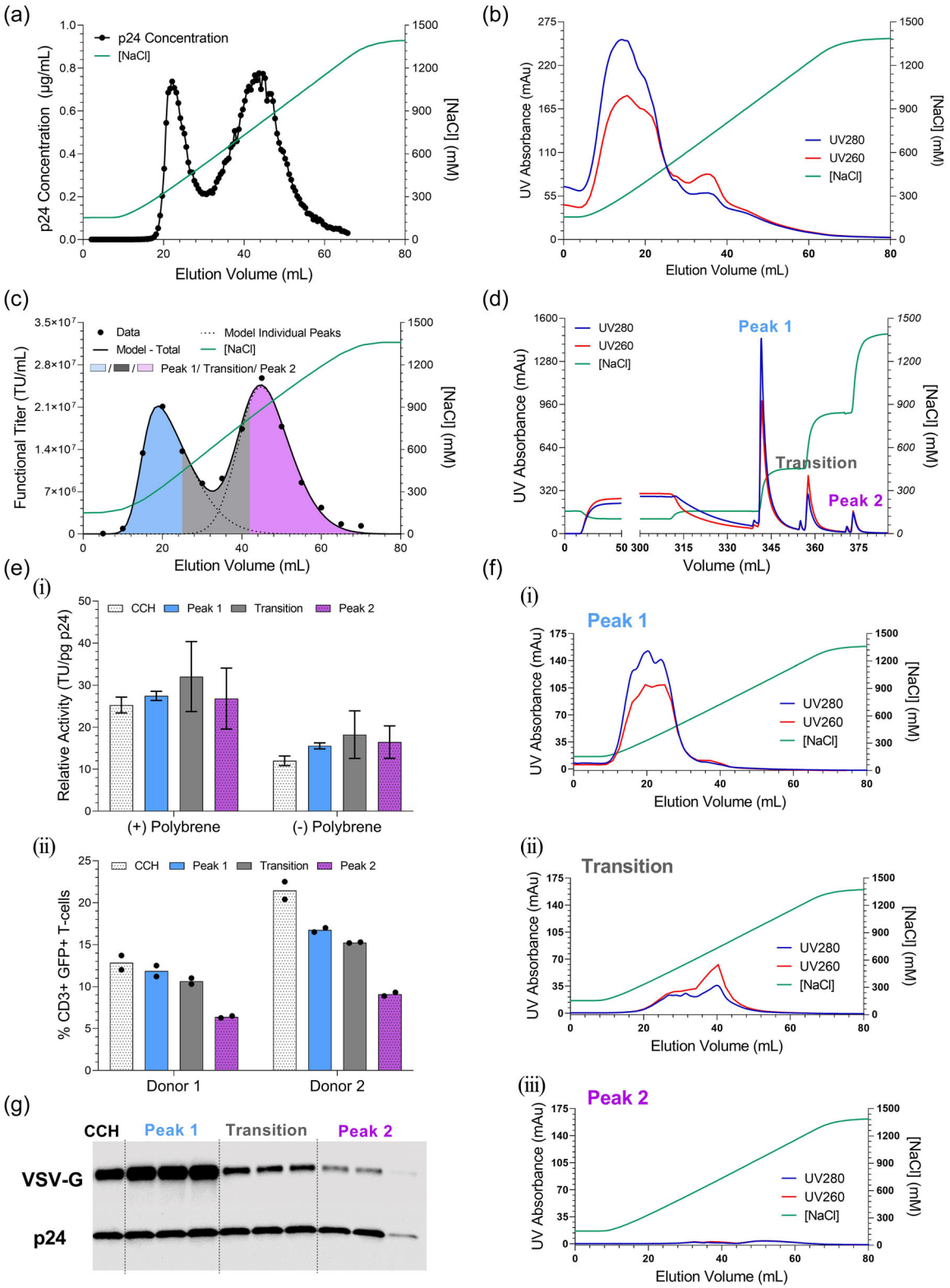

FIGURE 6 (See caption on next page).

3.8 | Reinjection of eluted LV populations onto AIEX chromatography

Two binding subpopulations could originate from either inter- or intraparticle envelope heterogeneity (Figure 1b). To test for the predominant mechanism, material from each peak was generated and subsequently re-injected back onto a new Q-membrane. If a two-peak profile is re-established upon reinjection of a single peak, this would evidence multiple binding domains on the vector envelope (intraparticle heterogeneity). If a single peak remains upon reinjection this would evidence discrete LV populations (interparticle heterogeneity) (Figure 1b). A gradient elution was initially conducted to establish the LV elution profile of this material (Figure 6b&c). The location of the underlying populations in the two-peak profile were estimated using the skewed-Gaussian model (Section 2.9) and are indicated on Figure 6c. Using this model, salt elution points that gave material from peak 1 (450 mM), the transition (825 mM) and peak 2 (1350 mM) could be defined (Figure 6c) and used in a subsequent step elution run to generate peak material (Figure 6d). Step elutions were conducted in triplicate with peaks immediately diluted to 150 mM NaCl and re-injected onto new Q-membranes followed by gradient elution (Figure 6f).

Figure 7a gives the p24 LV elution profile of the re-injected peak materials. Peak 2 elution displays a single peak (~1000 mM NaCl), consistent with its retention point in the gradient control (Figure 6c). Peak 1 also exhibits a single elution peak (~350 mM NaCl) consistent with the control. However, peak 1 also displays significant tailing with 25% of total eluted p24 appearing above the expected 450 mM NaCl cut off. This could result from mass transport effects but is perhaps more likely to stem from complex multistate binding. As the degree of multipoint attachment increases with extended adsorption duration, an apparent 'shift' in LV elution to higher salt would occur. This would not be observed for peak 2, as material effectively transitions to a 'third' irreversibly bound peak that is never recovered (Figure 1b). As anticipated, reinjection of the transition region, containing material from both peaks, re-establishes the two-peak profile. Functional titer profiles (Figure 7b) display near identical trends to that of p24 but with slightly lower titers observed at higher salt concentrations, likely due to functionality loss associated with high salt.

As reinjection of peak 1 and peak 2 LV material resulted in single peaks, and no re-establishment of a two-peak profile, these data support the hypothesis that the profile arises from distinct LV subpopulations in the CCH displaying interparticle envelope heterogeneity (Figure 1b,i). These findings have implications for upstream bioprocessing, as to what factors influence the emergence of different LV populations, but also highlight the need to stop considering LV product pools as homogenous target species during separation processes development.

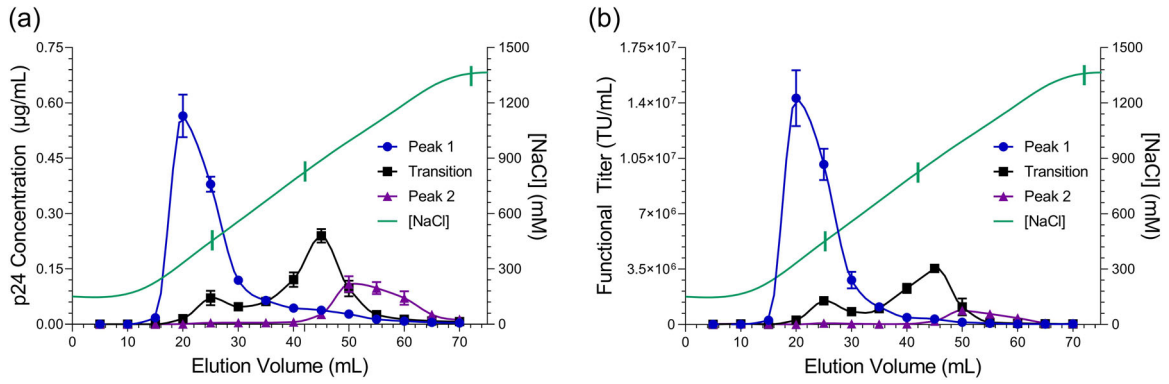

FIGURE 7 Elution profiles from the reinjection of each LV peak material. Error bars represent ±1 SD at $N = 3$ biological replicates. Vertical dashes represent the original NaCl step elution cut points. (a) p24 elution profile of each LV peak material after reinjection to the AIEX Q-membrane adsorber. (b) Functional titer elution profile of each LV peak material after reinjection to the AIEX Q-membrane adsorber.

FIGURE 6 Generation and reinjection of LV material obtained from different points of the two-peak elution profile. Peak 1 (blue), Transition (gray) and Peak 2 (pink). (a) High resolution LV p24 elution profile (0.5 CV sample resolution). (b) Chromatogram of elution window from the gradient elution control. (c) Functional titer elution profile obtained from the gradient control (p24 is not shown for clarity). Locations of both peaks were estimated from the skewed-Gaussian model described in Section 2.9. Estimated peak contents following 450 mM, 825 mM, and 1350 mM NaCl elutions are indicated by the shaded regions. (d) Representative chromatogram of the step elution used to generate material for Peak 1 (450 mM), Transition (825 mM) and Peak 2 (1350 mM). (e) Activity of each eluted LV fraction from the step elution. (i) Relative activity based on transduction of HEK293T cells with and without polybrene. Peak error bars represent ±1 SD at $N = 4$ biological replicates. (ii) Activity based on T-cell transduction of two donor cell populations at an MOI of 0.5. A single run is given with technical replicates indicated on figure. (f) Representative chromatogram of the elution window from the reinjection of each peak material onto a new Q-membrane adsorbers (i) Peak 1, (ii) Transition and (iii) Peak 2. (g) Western blot of VSV-G concentration in the CCH and each peak from the step elution. All fractions were normalized to the same p24 concentration based of the p24 ELISA read out. Thus, bands represent the relative VSV-G: p24 ratio. Columns contain $N = 3$ biological replicates. MOI, multiplicity of infection.

3.9 | Characterizing activity differences between elution peaks

Previous authors have documented differences in functionality between eluted LV peaks (Yamada et al., 2003). The relative activity of each peak was therefore calculated from the step elution material to try and infer potential structural difference between LV populations (Figure 6e,i). No significant difference in relative activity was detected when compared to the CCH (25.3 TU/pg p24) for peak 1 and peak 2 (27.5 & 26.8 TU/pg p24 respectively). Samples were also measured in the absence of polybrene, in case the transduction aid masked functionality differences, with a similar trend observed at overall lower activity (12.0, 15.6, and 16.5 TU/pg p24 respectively). VSV-G concentration, normalized to p24, was quantified by Western blot (Figure 6g) and shows a decrease in relative VSV-G concentration is observed from peak 1 to peak 2.

Despite observing no apparent difference in activity of peaks as measured by TU/pg p24 based upon transduction of HEK293T cells, we wished to see whether a similar pattern was observed on a real target cell line. Material from each peak was used to transduce T cells from two donors at an MOI of 0.5. The % CD3 + GFP + T cells reduced from 11.9% (peak 1) to 6.4% (peak 2) for Donor 1 and from 16.8% (peak 1) to 6.4% (peak 2) for Donor 2 giving a 1.85-fold decrease in relative transduction capability. These data could indicate that peak 2 LV material is less effective at transducing target cells, however the impact of different contaminant profiles cannot be ruled out. This aligns with previous work suggesting reduced activity of vector in peak 2 (Yamada et al., 2003).

3.10 | Relationship between postinduction harvest time and AIEX elution profile

The two-peak profile, stemming from interparticle envelope heterogeneity, is attributable to inherent structural differences between LV populations. This is likely linked to the cell culture environment, which defines the viral assembly conditions. Given that LV production negatively affects cell viability, and the density of certain HS proteoglycans in HEK293 membranes depends on the cell growth phase and viability, we hypothesized that the two-peak profile may simply arise from vector populations produced at different times during production due to differences in the budded cell membrane composition (Lee et al., 2016)

LV CCH was harvested at $t = 6$ h and $t = 24$ h post induction and this was conducted in triplicate. These times represent the earliest and latest points of vector production based on our previously reported cell culture processing times (Pamenter et al., 2023). Each CCH was then loaded onto Q-membranes (AIEX protocol, Section 2.2). Despite a drop in cell viability at harvest (94.8% −84.3%), a clear two-peak profile was observed at both harvest times which does not support the hypothesis (Figure 8). Further investigation is therefore needed to elucidate the specific cell culture factors behind these distinct binding populations.

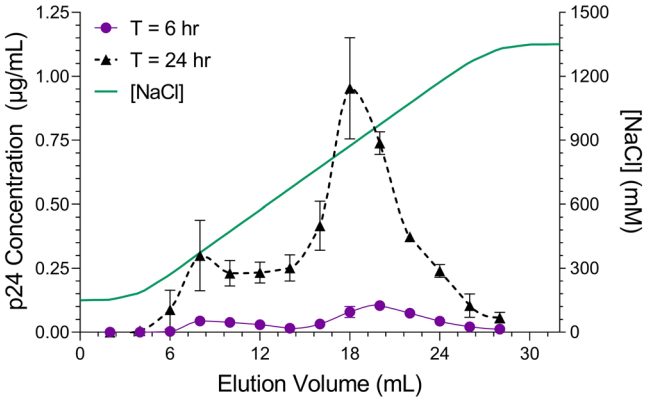

FIGURE 8 Impact of post induction harvest time on the two-peak gradient elution profile measured by p24 concentration. Error bars represent ±1 SD at $N = 3$ biological replicates.

4 | CONCLUSION

The results of this work identify the role specific LV envelope species play in defining LV AIEX binding and demonstrate what vector structural factors give rise to the heterogeneous two-peak elution profile. Initially, the role of the VSV-G pseudotype protein was investigated due to its hypothesized role in LV binding. LV preparations were generated with varying levels of VSV-G protein. The two-peak elution profile persisted across all LV VSV-G protein levels, including when VSV-G was completely absent, ruling it out as a major binding determinant.

To identify other envelope species potentially responsible for LV binding, we reviewed the fundamental composition of the LV glycocalyx and highlighted the presence of highly-charged glycosaminoglycans in membrane proteoglycans. LVs devoid of membrane VSV-G were subject to enzymatic digestion of envelope GAGs. Heparan Sulfate digestion alone significantly impacted the two-peak profile, reducing the proportion of eluted material recovered in peak 2 from 50% to 25%. Combined digestion of HS and Chondroitin Sulfate further decreased the peak 2 proportion to 3.1%, accompanied by a threefold increase in peak 1 maximum. These results support the hypothesis that envelope GAGs are major determinants of LV elution heterogeneity, causing strong interaction of LV in peak 2. The cause of peak 1 binding was not fully ascertained, but (-) VSV-G LV subjected to Tryp digestion were able to bind in this region. As this treatment should theoretically strip all proteinous envelope species, resulting in 'bald' LVs, this could suggest interaction through the phospholipid membrane. However, membrane proteins resistant to Tryp cannot be ruled out.

Having demonstrated the role of GAGs in binding (-) VSV-G LV, we ascertained whether similar behaviors were observed upon enzymatic digestion of HS and CS from functional LV containing VSV-G. A similar increase in peak 1, and reduction in peak 2, elution content was observed which demonstrates the role of GAGs in binding functional LV to the adsorbent. A moderate increase in TU recovery (18% to 42%) was also observed, though incubation alone

resulted in significant TU losses of 22%, making addition of GAG-digesting enzymes an unlikely option for improving LV AIEX.

We hypothesized that two peaks could have two origins (Figure 1b). Firstly, separate subpopulations of LV with different binding species in their envelope (interparticle envelope heterogeneity). Secondly, vectors possessing multiple binding domains on their surface with two peaks emerging from a stochastic process with binding mode determined by the orientation of LV upon surface contact (intraparticle envelope heterogeneity). Experiments isolating material from peak 1 and peak 2, and then re-injecting them onto AIEX adsorbents, resulted in single peaks with retention points consistent with the original two-peak profile.

These data support the hypothesis that discrete LV populations present in the cell culture lead to the two-peak profile (interparticle envelope heterogeneity). The origin of structural diversity in LV membranes is uncertain but may stem from factors such as LV-specific budding location or inter-cell transfection efficiency. Our data shows elevated levels of VSV-G are present in vectors eluted in peak 1, perhaps suggesting features associated with this form of virus are those involved with the adsorption mechanism. Although we determined VSV-G is not directly responsible, concentration of VSV-G in the envelope may be inversely correlated with that of GAG containing proteoglycans, resulting in a greater proportion of peak 2 binding for vectors possessing lower VSV-G envelope densities. This complexity underscores our limited understanding of envelope species arrangement at resolutions necessary for full mechanistic understanding of LV-AIEX ligand binding. Further research is needed to unravel the factors driving distinct LV populations with variable envelope compositions. These findings have broader implications beyond LV systems, as analogous behaviors are anticipated during charge-based separation of enveloped viruses, VLPs, or vesicles.

AUTHOR CONTRIBUTIONS

George Pamenter, Daniel G. Bracewell, Lee Davies, and Ciaran Lamont conceived the study. George Pamenter designed experiments. George Pamenter, Ciaran Lamont, and Danyal Rahim executed studies. Duygu Dikicioglu, Daniel G. Bracewell, and George Pamenter developed the analysis and modeling methodology. Research was performed in the laboratory of James Miskin, Kyriacos Mitrophanous, and Carol Knevelman. George Pamenter and Daniel G. Bracewell wrote the manuscript with contributions from all other authors.

ACKNOWLEDGMENTS

The research reported is affiliated with and supported by Oxford Biomedica (UK) Ltd. We thank the Engineering and Physical Sciences Research Council (EPSRC) for funding the Center for Doctoral Training in Bioprocess Engineering Leadership at UCL (Grant Ref: EP/S021868/1) and the Future Targeted Healthcare Manufacturing Hub in collaboration with UK universities and a consortium of industrial users and sector organizations (Grant Ref: EP/P006485/1). Collaboration and technical expertize from members of the Oxford Biomedica (UK) research departments are also thankfully acknowledged with specific recognition given to Mr Nathan Franklin, Dr. Anurag Kulkarni, Dr Magdalena Martin Urdiroz and Mr Thomas Williams. Special thanks are also given to the Oxford Biomedica (UK) Process Research & Development Analytics Team for the development and validation of the Ella™ high-throughput automated HIV-1 p24 ELISA which has enabled this work. Specific recognition here is given to Miss Donna Byrne, Miss Alison Fernandes and Miss Folashade Ogunrinade.

CONFLICT OF INTEREST STATEMENT

The authors declare no conflict of interest.

DATA AVAILABILITY STATEMENT

Data is available upon reasonable request to the author.

ORCID

George Pamenter http://orcid.org/0009-0009-9016-1716
Duygu Dikicioglu http://orcid.org/0000-0002-3018-4790
Daniel G. Bracewell http://orcid.org/0000-0003-3866-3304

REFERENCES

Alliance for Regenerative Medicine. (2023). *Cell and gene therapy sector data: Clinical trials*. https://alliancerm.org/data/

Bausch-Fluck, D., Hofmann, A., Bock, T., Frei, A. P., Cerciello, F., Jacobs, A., Moest, H., Omasits, U., Gundry, R. L., Yoon, C., Schiess, R., Schmidt, A., Mirkowska, P., Härtlová, A., Van Eyk, J. E., Bourquin, J. P., Aebersold, R., Boheler, K. R., Zandstra, P., & Wollscheid, B. (2015). A mass spectrometric-derived cell surface protein Atlas. *PLoS One*, *10*(4), e0121314. https://doi.org/10.1371/journal.pone.0121314

Beam Therapeutics. (2023). BEAM-201 Represents First Quadruplex-edited, Allogeneic CAR-T Cell Therapy Candidate in Clinical-stage Development and First Treatment with a Base Editing Candidate in United States, *Beam Therapeutics Announces First Patient Dosed in Phase 1/2 Trial of BEAM-201 in Relapsed, Refractory T-ALL/T-LL*. https://www.globenewswire.com/news-release/2023/09/05/2737092/0/en/Beam-Therapeutics-Announces-First-Patient-Dosed-in-Phase-1-2-Trial-of-BEAM-201-in-Relapsed-Refractory-T-ALL-T-LL.html

Binch, A. L. A., Shapiro, I. M., & Risbud, M. V. (2016). Syndecan-4 in intervertebral disc and cartilage: Saint or synner?, *Matrix Biology* (Vol. 52–54, pp. 355–362). Elsevier B.V. https://doi.org/10.1016/j.matbio.2016.01.005

Castelli, S., Young, R. M., & June, C. H. (2022). Off-the-shelf CAR T cells to treat cancer, In *Cell Research* (32(Issue 12), pp. 1036–1037). Springer Nature. https://doi.org/10.1038/s41422-022-00745-4

Comisel, R. M., Kara, B., Fiesser, F. H., & Farid, S. S. (2021). Lentiviral vector bioprocess economics for cell and gene therapy commercialization. *Biochemical Engineering Journal*, *167*, 107868. https://doi.org/10.1016/j.bej.2020.107868

Connell, B. J., & Lortat-Jacob, H. (2013). Human immunodeficiency virus and heparan sulfate: From attachment to entry inhibition. *Frontiers in Immunology*, *4*(Issue NOV), Article 385. https://doi.org/10.3389/fimmu.2013.00385

Couchman, J. R., & Pataki, C. A. (2012). An introduction to proteoglycans and their localization. *Journal of Histochemistry & Cytochemistry*, *60*(12), 885–897. https://doi.org/10.1369/0022155412464638

Dautzenberg, I. J. C., Rabelink, M. J. W. E., & Hoeben, R. C. (2021). The stability of envelope-pseudotyped lentiviral vectors. *Gene Therapy*, *28*(1–2), 89–104. https://doi.org/10.1038/s41434-020-00193-y

Diedrich, J., Heymann, W., Leweke, S., Hunt, S., Todd, R., Kunert, C., Johnson, W., & von Lieres, E. (2017). Multi-state steric mass action model and case study on complex high loading behavior of mAb on ion exchange tentacle resin. *Journal of Chromatography A*, *1525*, 60–70. https://doi.org/10.1016/j.chroma.2017.09.039

Farley, D. C., Iqball, S., Smith, J. C., Miskin, J. E., Kingsman, S. M., & Mitrophanous, K. A. (2007). Factors that influence VSV-G pseudotyping and transduction efficiency of lentiviral vectors—In vitro and in vivo implications. *The Journal of Gene Medicine*, *9*(5), 345–356. https://doi.org/10.1002/jgm.1022

Gerlach, J. Q., & Griffin, M. D. (2016). Getting to know the extracellular vesicle glycome, In *Molecular BioSystems* (12(Issue 4), pp. 1071–1081). Royal Society of Chemistry. https://doi.org/10.1039/c5mb00835b

Ghosh, R., Koley, S., Gopal, S., Rodrigues, A. L., Dordick, J. S., & Cramer, S. M. (2022). Evaluation of lentiviral vector stability and development of ion exchange purification processes. *Biotechnology Progress*, *38*(6), e3286. https://doi.org/10.1002/btpr.3286

Iozzo, R. V., & Schaefer, L. (2015). Proteoglycan form and function: A comprehensive nomenclature of proteoglycans, In *Matrix Biology* (42, pp. 11–55). Elsevier. https://doi.org/10.1016/j.matbio.2015.02.003

Kim, V. N., Mitrophanous, K., Kingsman, S. M., & Kingsman, A. J. (1998). Minimal requirement for a lentivirus vector based on Human Immunodeficiency Virus Type 1. *In JOURNAL OF VIROLOGY*, *72*(Issue 1), 811–816.

Lee, S., Kim, M. G., Kim, N., Heo, W. D., & Lee, G. M. (2016). Heparan sulfate proteoglycan synthesis in CHO DG44 and HEK293 cells. *Biotechnology and Bioprocess Engineering*, *21*(3), 439–445. https://doi.org/10.1007/s12257-015-0688-6

Masri, F., Cheeseman, E., & Ansorge, S. (2019). Viral vector manufacturing: how to address current and future demands? *Cell and Gene Therapy Insights*, *5*(S5), 949–970. https://doi.org/10.18609/cgti.2019.104

Mátrai, J., Chuah, M. K., & Vandendriessche, T. (2010). Recent advances in lentiviral vector development and applications, In *Molecular Therapy* (18(Issue 3), pp. 477–490). Nature Publishing Group. https://doi.org/10.1038/mt.2009.319

Milone, M. C., & O'Doherty, U. (2018). Clinical use of lentiviral vectors, In *Leukemia* (32(Issue 7), pp. 1529–1541). Nature Publishing Group. https://doi.org/10.1038/s41375-018-0106-0

Moreira, A. S., Cavaco, D. G., Faria, T. Q., Alves, P. M., Carrondo, M. J. T., & Peixoto, C. (2021). Advances in Lentivirus Purification, In *Biotechnology Journal* (16(Issue 1)). Wiley-VCH Verlag. https://doi.org/10.1002/biot.202000019

Naldini, L., Blomer, U., Gallay, P., Ory, D., Mulligan, R., Gage, F. H., Verma, I. M., & Trono, D. (1996). *In vivo gene delivery and stable transduction of nondividing cells by a lentiviral vector*. https://www.science.org

Nguyen, D. H., & K Hildreth, J. E. (2000). Evidence for budding of human immunodeficiency virus type 1 selectively from Glycolipid-Enriched membrane lipid rafts. *In Journal Of Virology*, *74*(Issue 7), 3264–3272. https://journals.asm.org/journal/jvi

Pamenter, G., Davies, L., Knevelman, C., Miskin, J., Mitrophanous, K., Dikicioglu, D., & Bracewell, D. G. (2023). Time-dependent sorption behavior of lentiviral vectors during anion-exchange chromatography. *Biotechnology and Bioengineering*, *120*, 2269–2282. https://doi.org/10.1002/bit.28483

Perry, C., & Rayat, A. C. M. E. (2021). Lentiviral vector bioprocessing. *Viruses*, *13*(2), 268. https://doi.org/10.3390/v13020268

Philippidis, A. (2017). Virus Supply Vexes Gene Therapy Developers, CMOs, *Genetic Engineering and Biotechnology News*.

Rodrigues, T., Alves, A., Lopes, A., Carrondo, M. J. T., Alves, P. M., & Cruz, P. E. (2008). Removal of envelope protein-free retroviral vectors by anion-exchange chromatography to improve product quality. *Journal of Separation Science*, *31*(20), 3509–3518. https://doi.org/10.1002/jssc.200800195

Shi, D., Sheng, A., & Chi, L. (2021). Glycosaminoglycan-Protein Interactions and Their Roles in Human Disease, *In Frontiers in Molecular Biosciences* (Vol. 8). Frontiers Media S.A. https://doi.org/10.3389/fmolb.2021.639666

Srivastava, S., & Foster, J. (2023). The new economics of cell and gene therapy. *Cell & Gene*. https://www.cellandgene.com/doc/the-new-economics-of-cell-and-gene-therapy-0001

UniProt. (2024). *Vesicular stomatitis Indiana virus (strain San Juan) (VSIV) Glycoprotein—P03522 (GLYCO_VSIVA)*. https://www.uniprot.org/uniprotkb/P03522/entry

Valkama, A. J., Oruetxebarria, I., Lipponen, E. M., Leinonen, H. M., Käyhty, P., Hynynen, H., Turkki, V., Malinen, J., Miinalainen, T., Heikura, T., Parker, N. R., Ylä-Herttuala, S., & Lesch, H. P. (2020). Development of Large-Scale downstream processing for lentiviral vectors. *Molecular Therapy—Methods & Clinical Development*, *17*, 717–730. https://doi.org/10.1016/j.omtm.2020.03.025

Verma, M., Obergfell, K., Topp, S., Panier, V., & Wu, J. (2023). The next-generation CAR-T therapy landscape. *Nature Reviews Drug Discovery*, *22*, 776–777.

Vivès, R. R., Imberty, A., Sattentau, Q. J., & Lortat-Jacob, H. (2005). Heparan sulfate targets the HIV-1 envelope glycoprotein gp120 coreceptor binding site. *Journal of Biological Chemistry*, *280*(22), 21353–21357. https://doi.org/10.1074/jbc.M500911200

Xin, T., Cheng, L., Zhou, C., Zhao, Y., Hu, Z., & Wu, X. (2022). In-Vivo Induced CAR-T Cell for the Potential Breakthrough to Overcome the Barriers of Current CAR-T Cell Therapy, *In Frontiers in Oncology* (Vol. 12). Frontiers Media S.A. https://doi.org/10.3389/fonc.2022.809754

Yamada, K., McCarty, D. M., Madden, V. J., & Walsh, C. E. (2003). Lentivirus vector purification using anion exchange HPLC leads to improved gene transfer. *Biotechniques*, *34*(5), 1074–1080. https://doi.org/10.2144/03345dd04

Zheng, W., He, R., Liang, X., Roudi, S., Bost, J., Coly, P. M., van Niel, G., & Andaloussi, S. E. L. (2022). Cell-specific targeting of extracellular vesicles through engineering the glycocalyx. *Journal of Extracellular Vesicles*, *11*(12), 00. https://doi.org/10.1002/jev2.12290

How to cite this article: Pamenter, G., Davies, L., Lamont, C., Rahim, D., Knevelman, C., Miskin, J., Mitrophanous, K., Dikicioglu, D., & Bracewell, D. G. (2024). Lentiviral vector determinants of anion-exchange chromatography elution heterogeneity. *Biotechnology and Bioengineering*, *121*, 2936–2951. https://doi.org/10.1002/bit.28766